Analytic variational method for Hamiltonian lattice gauge theory in 3+1 dimensions

Ming C. Huang*
Department of Physics, University of Florida, Gainesville, Florida 32602

Mohammad W. Katoot†
Space Astronomy Laboratory, University of Florida, Gainesville, Florida 32609
(Received 14 June 1989; revised manuscript received 2 November 1989)

We present an analytic variational method in 3+1 dimensions for Hamiltonian lattice gauge theory. This method is based on Batrouni's mean-plaquette method and Robson's plaquette space integration. The Abelianized Bianchi identities are used and a detailed study of the number of identities that are needed and the validity of this approximation is given. The variational vacuum we use is the product of single-plaquette wave functions. The gauge group we consider here is SU(2), but the method is valid for any gauge theory. We apply this method to calculate the 0^{++} glueball mass, and, in addition, the results of the string tension (scaling is observed) and its roughening transition are presented.

I. INTRODUCTION

It is strongly believed among physicists that quantum chromodynamics is the underlying theory of strong interactions. This theory exhibits two distinctive features. At short distances it is asymptotically free;[1] the effective coupling constant is small, and thus the interactions can be analyzed using perturbative methods. This feature has made possible the explanation of the approximate scaling seen in deep-inelastic scattering of leptons on hadrons,[2] and many other confirmations of perturbative QCD calculations at high energy. On the other hand, the theory exhibits confinement.[1,3] At large distances, the effective coupling is large which prohibits the use of perturbation theory. Several nonperturbative approaches have been utilized to study this complicated low-energy region of the theory, among the most successful is lattice gauge theory.[3] Two different methods are used in lattice gauge theory. (a) Numerical simulation. Various Monte Carlo techniques have provided many indispensable results,[4] partially clarifying the dynamics of the theory, and giving numerical values of different physical quantities. However, these studies cannot yield an understanding of the important field configurations that contribute to the physics of the problem at hand, such as the vacuum structure which is believed to be responsible for confinement and chiral-symmetry breaking. In addition, inclusion of the dynamical fermions and problems related to finite-size effects require prohibitively long CPU time, which sometimes forces severe approximations.[5] (b) Analytical methods. These are divided into two categories: (i) strong-coupling expansion[6] (SCE) and (ii) variational methods in the Hamiltonian formulation.[7,8] In the former, one starts in the strong-coupling regions and develops a perturbation expansion in $1/g$; then the Padé approximation techniques are utilized to extrapolate to the weak-coupling region. Although this method has revealed several important results and provided the test ground for other techniques, it becomes questionable in the weak-coupling region. Moreover, the existence of transitions such as the roughening transition prevents this method from making reliable conclusions beyond the transition coupling. On the other hand, variational techniques in the Hamiltonian formulation of lattice field theories avoid these drawbacks; they are suitable to study the dynamics over the whole range of the coupling constant (even in the presence of transitions), they provide considerable information about the important gauge field configurations, thus a better understanding of the physical phenomena, and at least for the gauge sector (as will be shown in this paper) analytical solutions are possible. The variational methods however have their own problems. They can only predict estimates of the various physical quantities (uncontrollable errors) and they are very complex. The first of these problems can be circumvented by changing the trial variational wave functions to include higher correlations. The second problem has driven some researchers to perform the calculations in 2+1 dimensions.[7,8] This is because, in 2+1 dimensions, one can transform the multidimensional integrals in link space to an integral in plaquette space, and the Jacobian of the transformation is the identity (this transformation is needed since the trial wave functions are functions of the various plaquettes). Thus the different matrix elements involved become essentially one-dimensional integrals.

In 3+1 dimensions, however, the Jacobian of the transformation is the lattice Bianchi identities, which set in correlations (actually, the major source of plaquette correlations comes from the Bianchi identity) between the different plaquettes and thus prevents an exact solution.

In this paper, we will present an analytic variational method in 3+1 dimensions for Hamiltonian SU(2) lattice gauge theory.[9] This work is based on Batrouni's mean-plaquette method[10] and Robson's plaquette space integra-

tion.[11] The trial ground state used is the product of single-plaquette wave functions, and the Bianchi identities are expanded in terms of characters of the group representations. A systematic study of the number of Bianchi identities needed and the convergence of the above expansion will be given in Sec. II. In Sec. III we present the analytic solution and apply it particularly to calculate the ground-state energy density, the string tension, and the roughening transition. In Sec. IV we apply this method also to calculate the 0^{++} glueball mass and finally Sec. V is devoted to conclusion and discussion.

II. SYSTEMATIC STUDY OF PLAQUETTE SPACE INTEGRATION

In this section we will review the transformation from link space to plaquette space, and then present a detailed analysis of the number of Bianchi identities that are sufficient for convergence. Although the work done here is in the Hamiltonian formalism for SU(2) lattice gauge theory, these techniques are easily extendable to the Lagrangian formalism and to any gauge group. The Kogut-Susskind Hamiltonian[12] for the SU(2) gauge group is

$$H=\frac{g_H^2}{2a}\sum_k\sum_a E_k^a E_k^a+\frac{2}{ag_H^2}\sum_p(2-\mathrm{tr}U_p)\ , \tag{2.1}$$

where a is the lattice spacing, g is the bare coupling constant, U_p is a SU(2) matrix associated with the plaquette p, and E_k^a is the color-electric-field operator which satisfies

$$[E_k^a,U_{k'}]=\delta_{kk'}\frac{\tau^a}{2}U_k\ , \tag{2.2}$$

where τ^a are the Pauli matrices.

For the trial ground-state wave function, we use the product of single-plaquette wave functions

$$\Phi_0=\exp\left[\lambda\sum_p\mathrm{tr}U_p\right]=\prod_p\exp(\lambda\,\mathrm{tr}U_p)\ , \tag{2.3}$$

where λ is a variational parameter. This wave function is exact in the strong-coupling region and it has been argued that it is reasonable in the intermediate coupling since the magnetic fluctuations of the ground state are quite localized.[13]

Since the physically relevant states are those which are gauge invariant, the various observables are functions of the traces of the different kinds of plaquettes. Therefore when calculating the different physical quantities, one needs to evaluate integrals of the form

$$\langle O(U_p)\rangle=\frac{\int[DU_l]\psi^\dagger(U_p)O(U_p)\psi(U_p)}{\int[DU]\psi^\dagger(U_p)\psi(U_p)}\ , \tag{2.4}$$

where $O(U_p)$ is the physical observable in question and $[DU_l]$ is the Haar measure in link space. This integral form is quite similar to those evaluated in the Lagrangian formulation of lattice gauge theory, except for the fact that the Haar measure here is defined over the three spatial coordinates rather than the four Euclidean space and time coordinates. A transformation from link space to plaquette space is clearly desirable, since it renders the integrand above to depend on the same variables. The first step toward this was taken by Halpern,[14] who constructed a unique inversion $A(F)$ for the potential A_μ in terms of the field strength $F_{\mu\nu}$ using a completely fixed axial-like gauge in continuum gauge theories with $F_{\mu\nu}$ constrained to satisfy the Bianchi identities

$$I_\nu\equiv D^\mu\tilde{F}_{\mu\nu}=0 \tag{2.5}$$

(it was pointed out by Halpern that the third Bianchi identity need not be satisfied at all points but only at a point $z=z_0$), where $\tilde{F}_{\mu\nu}\equiv\frac{1}{2}\epsilon_{\mu\nu\alpha\beta}F^{\mu\nu}$ is the dual field strength (when fixing the gauge, A_μ has two degrees of freedom, while $F_{\mu\nu}$ has six degrees of freedom, thus the four Bianchi identities are needed for a unique inversion). Therefore in general

$$\int[DA_\mu]\delta(CFG)f(F_{\mu\nu})=\int[DF_{\mu\nu}]\delta[I(F_{\mu\nu})]f(F_{\mu\nu})\ , \tag{2.6}$$

where $\delta(CFG)$ is a product of δ functions which fixes the gauge, and $\delta[I(F_{\mu\nu})]$ is the δ function which imposes the Bianchi-identity constraint.

The lattice version of this method was worked out by Batrouni,[15] who transformed the measure in Eq. (2.4) from link variables to plaquette variables, with the Jacobian of the transformation being the lattice Bianchi identities. Thus

$$\begin{aligned}\langle O(U_p)\rangle&=\frac{\int[DU_l]\psi^\dagger(U_p)O(U_p)\psi(U_p)}{\int[DU_l]\psi^\dagger(U_p)\psi(U_p)}\\&=\frac{\int[DU_p]\prod_c\delta(P_c-1)\psi^\dagger(U_p)O(U_p)\psi(U_p)}{\int[DU_p]\prod_c\delta(P_c-1)\psi^\dagger(U_p)\psi(U_p)}\ ,\end{aligned} \tag{2.7}$$

where $\delta(P_c-1)$ is the δ function of the non-Abelian lattice Bianchi identitiy for a given cube C. Under appropriate change of variables, these identities can be Abelianized (i.e., put in a form similar to those of Abelian gauge groups) with the result that

$$\delta(P_c-1)\rightarrow\delta(\bar{P}_c-1)=\delta\left[\prod_{i=1}^{6}\tilde{U}_p(i)-1\right]\ , \tag{2.8}$$

where $\tilde{U}_p(i)$ are the six plaquettes forming the cube C and the orientation is assumed to be taken into account properly. Notice that in Eq. (2.7) the Haar measure is defined in three spatial dimensions, so that the above Jacobian is the three spatial components of the lattice Bianchi identities in the Hamiltonian formalism.

The above "Abelianizing" transformation cannot be carried out over the entire lattice, but over a finite large region of it. This is not a severe drawback since, as discussed earlier, the vacuum magnetic fluctuations are quite localized, thus it suffices to work in a local region where the Bianchi identities are Abelianized and to

neglect the non-Abelianized identities since they usually occur in several lattice spacing units away from the local region (we shall justify this assumption below). This property permits the use of a small number of the Bianchi identities (small number of boxes), which in turn makes the calculation manageable. Robson[11] used this fact and used a character expansion of the identities and of the wave function to obtain an analytical method. Here we shall modify this method using the mean-plaquette approximation of Batrouni[10] for the gauge group SU(2), and compare its convergence to that of Robson. The SU(2) group structure is simple. Matrix elements of SU(2) can be parametrized as

$$U_p=\cos\left[\frac{\rho}{2}\right]-i\mathbf{n}\cdot\tau\sin\left[\frac{\rho}{2}\right], \tag{2.9}$$

where τ are the Pauli matrices and $\mathbf{n}$ is a three-dimensional unit vector. The character of the jth representation, denoted by $\chi_j(U_p)$, is

$$\chi_j(U_p)=\sum_{m=-j}^{j}\exp(im\rho)=\frac{\sin[(j+\frac{1}{2})\rho]}{\sin\left[\frac{\rho}{2}\right]} \tag{2.10a}$$

with the properties

$$\int dU_p\chi_j(U_p)\chi_k(U_p)=\delta_{j,k}\quad\text{(orthonormality)}, \tag{2.10b}$$

$$\chi_j(U_p)\chi_k(U_p)=\sum_{m=|j-k|}^{j+k}\chi_m(U_p). \tag{2.10c}$$

The trace of a plaquette is taken in the fundamental representation. Thus

$$\mathrm{tr}U_p=\chi_{1/2}(U_p)=2\cos\left[\frac{\rho}{2}\right]. \tag{2.11}$$

Inspecting Eq. (2.7), one can see that in the second equality the Haar measure and the wave functional are both invariant under the similarity transformations

$$U_p\to VU_pV^\dagger,$$

where $V\in$SU(2). Using this, the Abelianized Bianchi identities can be written as a series of separable products (using a character expansion for the identities and the Gross-Witten trick):

$$\delta(\tilde{P}_c-1)=\sum_j\frac{1}{(2j+1)^4}\prod_{i=1}^{6}\chi_j(U_{p_i}),\quad j=0,\tfrac{1}{2},1,\ldots$$
$$=1+\sum_j\frac{1}{(2j+1)^4}\left[\prod_{i=1}^{6}\chi_j(U_{p_i})\right],$$
$$j=\tfrac{1}{2},1,\tfrac{3}{2},\ldots. \tag{2.12}$$

The plaquette space integration method can be summarized as follows: starting with Eq. (2.7), keep a few number of Bianchi identities and character expand each of them as done in Eq. (2.12). A similar expansion is used for the trial vacuum and then the integration is carried out. We will first examine the expectation value for an elementary plaquette, using the trial vacuum (2.3):

$$\langle\mathrm{tr}U_p\rangle=\frac{\int[DU_p]\psi^\dagger(U_p)\chi_{1/2}(U_p)\psi(U_p)\prod_c\delta(P_c-1)}{\int[DU_p]\psi^\dagger(U_p)\psi(U_p)\prod_c\delta(P_c-1)}. \tag{2.13}$$

The questions to be addressed now are as follows. According to the above discussion, it suffices to include only a few number of Bianchi identities in order to obtain the correct value for (2.13). But how many identities are sufficient? Also if one uses Eq. (2.12) to expand these identities, at which value of j should one truncate?

To answer these questions, we start first with two Bianchi identities and study the convergence of the expansion (2.12), then the number of identities is increased to twelve and a similar convergence test is applied. Finally we use the mean-plaquette method for the above two cases and we compare to known Monte Carlo simulations for the 12 Bianchi identities case. Keeping two Bianchi identities [Fig. 1(a)] in Eq. (2.13) we have

$$\langle\mathrm{tr}U_p\rangle=\frac{\int\left[\prod_{i=1}^{11}dU_{p_i}\right]\left[\sum_{j_1}\sum_{j_2}\frac{1}{(2j_1+1)^4}\frac{1}{(2j_2+1)^4}\chi_{j_1}(U_{p_1})\chi_{j_2}(U_{p_1})\left[\prod_{k=2}^{6}\chi_{j_1}(U_{p_k})\right]\left[\prod_{n=7}^{11}\chi_{j_2}(U_{p_n})\right]\right](\mathrm{tr}U_{p_1})\prod_{m=1}^{11}\exp(2\lambda\,\mathrm{tr}U_{p_m})}{\int\left[\prod_{i=1}^{11}dU_{p_i}\right]\left[\sum_{j_1}\sum_{j_2}\frac{1}{(2j_1+1)^4}\frac{1}{(2j_2+1)^4}\chi_{j_1}(U_{p_1})\chi_{j_2}(U_{p_1})\left[\prod_{k=2}^{6}\chi_{j_1}(U_{p_k})\right]\left[\prod_{n=7}^{11}\chi_{j_2}(U_{p_n})\right]\right]\prod_{m=1}^{11}\exp(2\lambda\,\mathrm{tr}U_{p_m})}. \tag{2.14}$$

To evaluate the right-hand side of Eq. (2.14) notice that, apart from the measure and the factor $\exp(2\lambda\,\mathrm{tr}U_{p_m})$, the numerator and the denominator are powers of the different characters, and thus different powers of $\mathrm{tr}U_p$. On the other hand, notice that, in 2+1 dimensions,

$$\langle t_p\rangle\equiv\langle\mathrm{tr}U_p\rangle=\frac{\int dU_p(\mathrm{tr}U_p)\exp(2\lambda\,\mathrm{tr}U_p)}{\int dU_p\exp(2\lambda\,\mathrm{tr}U_p)}$$
$$=-\frac{1}{\lambda}+2\frac{I_0(4\lambda)}{I_1(4\lambda)}, \tag{2.15}$$

where $I_n(4\lambda)$ are the modified Bessel functions of order n. Differentiating this continuously with respect to 2λ, one obtains the expectation values of the various powers of $\mathrm{tr}U_p$. It is therefore straightforward (but cumbersome) to evaluate Eq. (2.14); this is done in Appendix A.

To study the convergence when j is truncated at some value, we define the quantity B:

$$B\equiv\frac{\langle O(U_p)\rangle_{3D}-\langle O(U_p)\rangle_{2D}}{\langle O(U_p)\rangle_{2D}}, \tag{2.16}$$

where the subscripts 2D and 3D denote the expectation

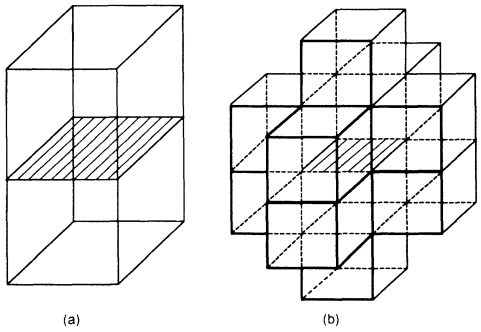

FIG. 1. A plaquette with (a) two Bianchi identities and (b) with twelve identities.

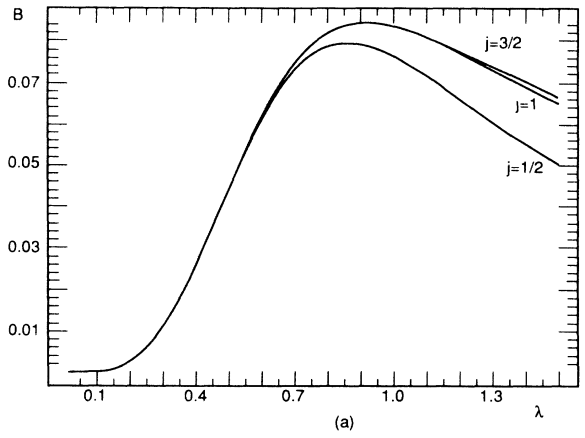

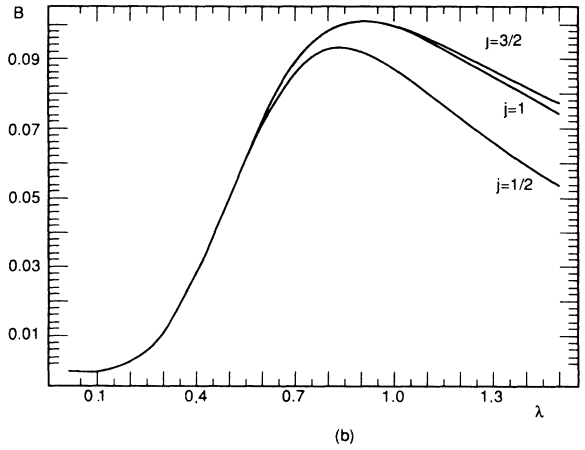

FIG. 2. (a) The B curves of the expectation value of a plaquette with two Bianchi identities. (b) The same but with 12 identities included.

values in 2 and 3 dimensions, respectively.

It is clear from Eq. (2.16) that B signifies the effects of the Bianchi identities; therefore, we can study the convergence of the expansion (2.12) in j by calculating B for different j values (for a fixed number of identities). B vs λ is plotted in Fig. 2(a) for different j values, where one can see clearly convergence occurring at $j=1$ for most of the λ range (this range corresponds to $0.1 \leq 1/2g2 \leq 0.5$). A similar curve is shown in Fig. 2(b), where 12 Bianchi identities are included [Fig. 1(b)]. Again here one can see that convergence is excellent for $j=1$ in the interesting region of the coupling constant. Shown in Fig. 3 is a comparison for $j=1$ for the two B curves in Figs. 2(a) and 2(b) (i.e., for 2 and 12 identities, respectively, and also 12 identities using the mean-plaquette approximation; see below). Clearly the difference is pronounced, and the question of a sufficient number of identities is yet to be settled. Instead of increasing the number of identities we shall now apply the mean-plaquette approximation and compare it directly to our previous Monte Carlo calculations.[16] The mean-plaquette approximation[10] is obtained by replacing the surface plaquettes in Eq. (2.13) by their expectation values:

$$\chi_j(U_p)=U_{2j}[\tfrac{1}{2}\mathrm{tr}U_p]\rightarrow U_{2j}[\tfrac{1}{2}\langle \mathrm{tr}U_p\rangle] ,$$

where U_{2j} is the Chebyshev polynomial of the second kind, and the integration in (2.13) is done then only over the internal plaquettes. The result of this calculation is, for the two-box approximation,

$$P(\lambda)=\frac{\sum_{j_1 j_2}\frac{1}{(2j_1+1)^4(2j_2+1)^4}U^5_{2j_1}(\frac{1}{2}P(\lambda))U^5_{2j_2}(\frac{1}{2}P(\lambda))N(j_1,j_2,\lambda)}{\sum_{j_3 j_4}\frac{1}{(2j_3+1)^4(2j_4+1)^4}U^5_{2j_3}(\frac{1}{2}P(\lambda))U^5_{2j_4}(\frac{1}{2}P(\lambda))M(j_3,j_4,\lambda)} ,$$

where

$$M(j_1,j_2,\lambda)=\sum_{k=|j_1-j_2|}^{j_1+j_2}(2k+1)I_{2k+1}(4\lambda)$$

and

$$N(j_1,j_2,\lambda)=\sum_j\sum_{k=|j_1-j_2|}^{j_1+j_2}\sum_{|p=|j-k|}^{j+k}(2j+1)I_{2j+1}(4\lambda)\delta_{p,1/2} \tag{2.17}$$

and, for the 12-box approximation,

$$P(\lambda)=\frac{\sum_{j_1}\sum_{j_2}\frac{1}{(2j_1+1)^4}\frac{1}{(2j_2+1)^4}M[j_1,j_2,\lambda]Q^4[j_1,j_2,\lambda,P(\lambda)]R[j_1,j_2,\lambda,P(\lambda)]}{\sum_{j_1}\sum_{j_2}\frac{1}{(2j_1+1)^4}\frac{1}{(2j_2+1)^4}N[j_1,j_2,\lambda]Q^4[j_1,j_2,\lambda,P(\lambda)]R[j_1,j_2,\lambda,P(\lambda)]},$$

where

$$P(\lambda)=\langle \mathrm{tr}U_p\rangle ,$$

$$N[j_1,j_2,\lambda]=\sum_{j=|j_1-j_2|}^{j_1+j_2}(2j+1)I_{2j+1}(4\lambda) ,$$

$$M(j_1,j_2,\lambda)=\sum_j\sum_{k=|j_1-j_2|}^{j_1+j_2}\sum_{p=|j-k|}^{j+k}(2j+1)I_{2j+1}(4\lambda)\delta_{p,1/2}N[j_1,j_3,\lambda]N[j_2,j_4,\lambda]N[j_3,j_4,\lambda] ,$$

$$Q[j_1,j_2,\lambda,P(\lambda)]=\sum_{j_3}\sum_{j_4}\frac{1}{(2j_3+1)^4}\frac{1}{(2j_4+1)^4}U^4_{2j_3}[\tfrac{1}{2}P(\lambda)]U^4_{2j_4}[\tfrac{1}{2}P(\lambda)]N[j_1,j_3,\lambda]N[j_2,j_4,\lambda]N[j_3,j_4,\lambda] ,$$

and

$$R[j_1,j_2,\lambda,P(\lambda)]=\sum_{j_3}\sum_{j_4}\frac{1}{(2j_3+1)^4}\frac{1}{(2j_4+1)^4}U^5_{2j_3}[\tfrac{1}{2}P(\lambda)]U^5_{2j_4}[\tfrac{1}{2}P(\lambda)]N[j_1,j_3,\lambda]N[j_2,j_4,\lambda] . \quad (2.18)$$

We leave the derivation of Eqs. (2.17) and (2.18) to Appendix A as well.

Using Eq. (2.17) for the expectation value of $\mathrm{tr}U_p$, B is plotted in Fig. 4 for different j values and using 12 Bianchi identities, where again convergence is seen to occur at $j=1$. Figure 3 compares the different B curves including two identities, 12 identities, and 12 identities using the mean-plaquette approximation. It is clear that the latter approximation is better than the other two (remember that B indicates the difference between the expectation values in $3+1$ and $2+1$ dimensions). To confirm this, we compare in Table I the expectation value of an elementary plaquette using 12 Bianchi identities in the mean-plaquette approximation with our Monte Carlo result.[16] We also compared these results with the exact calculation of Chin *et al.*[17] (not shown in the table); the agreement in both cases is excellent.

We have carried out this analysis one step further, by looking at the expectation value of a planar extended plaquette containing two elementary plaquettes. In this case the proper number of identities is four for the first approximation (two on the top and two on the bottom to cover the two elementary plaquettes), and then 20 identities to cover the above four. For the 20 Bianchi identities, the expectation value of the extended plaquette using the mean-plaquette approximation is

$$\langle \mathrm{tr}(U_{p_1}U_{p_2})\rangle$$

$$=\frac{1}{2}\frac{\sum_{j_1}\sum_{j_2}\sum_{j_3}\sum_{j_4}\left[\prod_{i=1}^{4}\frac{1}{(2j_i+1)^4}\right]M[j_1,j_2,\lambda]M[j_3,j_4,\lambda]N[j_1,j_3,\lambda]N[j_2,j_4,\lambda]S^2[j_1,j_2,j_3,j_4,\lambda,P(\lambda)]Q[j_1,j_2,j_3,j_4,\lambda,P(\lambda)]}{\sum_{j_1}\sum_{j_2}\sum_{j_3}\sum_{j_4}\left[\prod_{i=1}^{4}\frac{1}{(2j_i+1)^4}\right]N[j_1,j_2,\lambda]N[j_3,j_4,\lambda]N[j_1,j_3,\lambda]N[j_2,j_4,\lambda]S^2[j_1,j_2,j_3,j_4,\lambda,P(\lambda)]Q[j_1,j_2,j_3,j_4,\lambda,P(\lambda)]} \quad (2.19)$$

where

$$S[j_1,j_2,j_3,j_4,\lambda,P(\lambda)]=\sum_{k_1}\sum_{k_2}\sum_{k_3}\sum_{k_4}\left[\prod_{i=1}^{4}\frac{U^3_{2k_i}[\frac{1}{2}P(\lambda)]}{(2k_i+1)^4}\right]N[j_1,k_1,\lambda]$$
$$\times N[j_2,k_2,\lambda]N[j_3,k_3,\lambda]N[j_4,k_4,\lambda]N[k_1,k_2,\lambda]$$
$$\times N[k_3,k_4,\lambda]N[k_1,k_3,\lambda]N[k_2,k_4,\lambda] ,$$

$$T[j_1,j_2,\lambda,P(\lambda)]=\sum_{k_1}\sum_{k_2}\left[\prod_{i=1}^{2}\frac{U^4_{2k_i}[\frac{1}{2}P(\lambda)]}{(2k_i+1)^4}\right]N[j_1,k_1,\lambda]N[j_2,k_2,\lambda]N[k_1,k_2,\lambda] .$$

and

$$Q[j_1,j_2,j_3,j_4,\lambda,P(\lambda)]=T[j_1,j_2,\lambda,P(\lambda)]T[j_3,j_4,\lambda,P(\lambda)]T[j_1,j_3,\lambda,P(\lambda)]T[j_2,j_4,\lambda,P(\lambda)] .$$

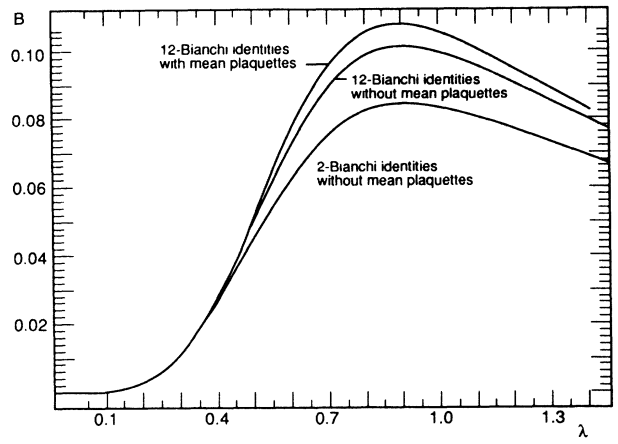

FIG. 3. A comparison between the B curves of 2 and 12 identities, and 12 identities with the mean-plaquette approximation.

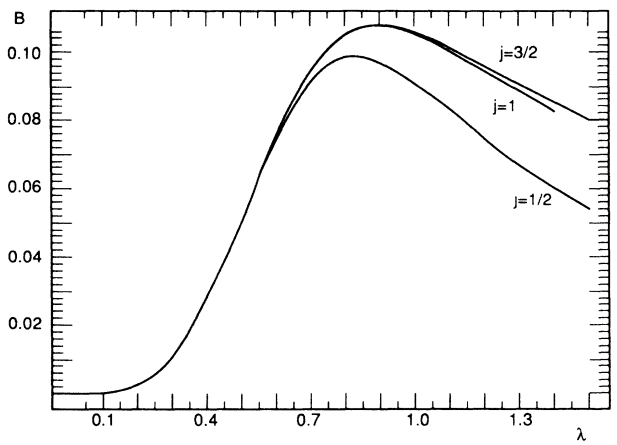

FIG. 4. The B curves for 12 identities using mean-plaquette approximation.

In this case we also find that $j=1$ is the appropriate cutoff in (2.20). Figure 5 shows the B curve for the cases of four Bianchi identities without using the mean-plaquette approximation, 20 identities without using the mean-plaquette approximation, and 20 identities with the mean-plaquette approximation. A similar behavior to that of the expectation value of an elementary plaquette is seen here, which indicates that the latter approximation (20 identities with the mean-plaquette approximation) is sufficient. This has also been confirmed by comparing it to our Monte Carlo calculation.[16]

Let us now summarize this section and discuss a few important points. The expectation value of any plaquette can be calculated to a very good accuracy by covering that plaquette with Bianchi identities (two in the case of an elementary plaquette and four for the planar extended plaquette discussed above). These identities (boxes) in turn should also be covered completely with Bianchi identities (thus resulting in 12 identities for the elementary plaquette and 20 identities for the planar extended plaquette). The mean-plaquette approximation is then utilized by which all the surface plaquettes are replaced by their expectation values and the integration is only carried out for the internal plaquettes (this results in a self-consistent solution for the expectation values). We have shown in the various examples worked out here that it suffices to truncate the character expansion of the identities at the adjoint representation for SU(2). The excellent agreement with Monte Carlo calculations shows that neglecting the non-Abelianized Bianchi identities is justifiable, and that in turn is more evidence of the local nature of the ground-state magnetic fluctuations.

Finally, examining all the B curves presented in this section one can see a clear systematic behavior of B as a function of the variational parameter. At small λ (strong coupling) it approaches zero as it should, since in this region plaquette disorder dominates (here the correlations set in by the Bianchi identities vanish; this agrees with Batrouni's[10] conclusion that the strong-coupling expansion can be seen as a gradual restoration of the Bianchi

TABLE I. A comparison between the results of our analytic method and the Monte Carlo simulation reported in Ref. 16.

2λ	Analytical calculation	Monte Carlo simulation
0.197(1)	0.195 871	0.1964(08)
0.262(1)	0.259 291	0.2592(08)
0.326(1)	0.320 871	0.3194(08)
0.393(2)	0.384 410	0.3848(08)
0.453(2)	0.440 293	0.4404(08)
0.516(4)	0.498 193	0.4970(10)
0.583(4)	0.558 514	0.5572(12)
0.646(3)	0.614 177	0.6116(12)
0.699(3)	0.660 372	0.6632(12)
0.763(4)	0.715 391	0.7140(14)
0.893(8)	0.824 369	0.8148(14)
0.996(5)	0.907 089	0.9056(16)
1.091(7)	0.980 752	0.9810(16)
1.186(7)	1.050 616	1.0516(24)
1.385(5)	1.181 302	1.1830(10)
1.554(5)	1.272 673	1.2770(10)

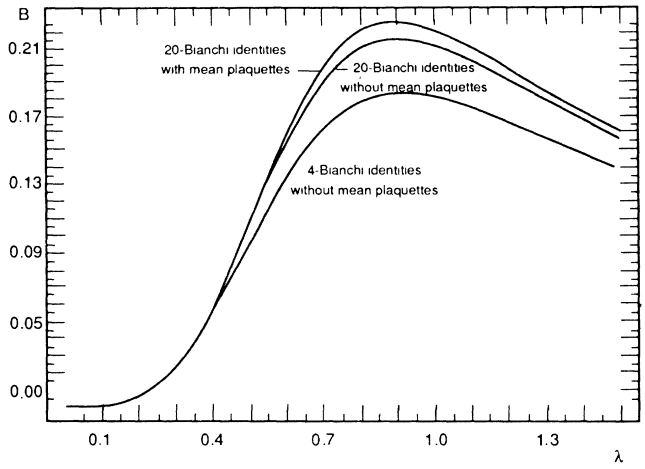

FIG. 5. The different B curves for an extended plaquette described in the text.

identities). As λ increases (intermediate coupling), the B curves rise rapidly (signaling correlations due to the Bianchi identities) until they reach a maximum which is followed by a decline at about $\lambda=0.9$ (or $1/2g^2=0.38$) in the weak-coupling region. This last fall off indicates a poor trial vacuum in the weak-coupling region; a problem which has been reported by several authors.[7,8,18] Nevertheless, from the B curves presented here one may conclude that the trial vacuum may be adequate in the scaling region (intermediate coupling). This problem will arise later in the next sections and we will have more to say about it there.

III. APPLICATIONS

A. The static quark-antiquark potential

In this section we will apply the methods developed in the previous section to various physical quantities. We start with the static quark-antiquark potential. Some of the results of these calculations have been reported elsewhere;[19] however, here we shall display the details of the calculations.

The emergence of the flux-tube picture, as a physical picture of confinement (i.e., the flux between a quark and an antiquark is confined in a tube) has triggered several studies to understand their dynamics. Analysis of the dynamics of structureless tubes (strings) in the long-wavelength regime revealed that the heavy-quark potential has, in addition to the linear confining term, power corrections (due to the zero-mass fluctuations of the string),

$$V(R)=\alpha R+\beta+\gamma R^{-1}+O(R^{-2}) ,$$

where γ is a universal constant depending only on the space-time dimension. Another important result due to these massless modes is that the string is delocalized (roughens in the long-wavelength limit). On the lattice, Kogut *et al.*[20] investigated the heavy-quark potential and the string dynamics by considering off-axis strings. Their study has yielded the following results: (a) The off-axis strings are rough for all couplings (i.e., the string experiences unbounded transverse fluctuations); (b) similar to the continuum case, the potential has power corrections due to the absence of a mass gap in the string's spectrum, and the Coulomb term has a universal coefficient; and (c) roughening occurs when the kink mass (the energy difference between a straight string and a string with a transverse link) vanishes, at which point the equipotentials are (essentially) spheres. It is important to notice that these conclusions are drawn from analyzing the off-axis strings; the on-axis case does not yield, for example, a smooth crossover to the continuum limit due to the existence of two different phases: for $g>g_R$ the string does not fluctuate and for $g<g_R$ the string fluctuates and starts resembling its continuous analog. These analyses were carried out using the strong-coupling expansion. Another important result of this calculation was that the roughening transition occurred in the weak-coupling region, in contrast with the Lagrangian calculations which predict roughening at intermediate couplings (thus making it difficult to predict the continuum physics in the string sector). Using variational techniques in $2+1$ dimensions, Tonkin[8] analyzed the heavy-quark potential and calculated the string tension using different vacua. It was shown there that the equipotential surfaces remained smooth even after the roughening point in contrast to the strong-coupling results, due to the fact that the vacua utilized in the calculations are nontrivial. Here we shall carry out a similar analysis in $3+1$ dimensions using the methods developed in Sec. II.

An operator which describes a heavy quark (q)-antiquark ($\bar{q}$) pair which is invariant under the generalized color rotations

$$\sum_k E_k^a(\mathbf{n})\rightarrow\sum_k E_k^a(\mathbf{n})+\Psi^\dagger(\mathbf{n})\frac{\tau^a}{2}\Psi(\mathbf{n}) \tag{3.1}$$

is

$$\Psi^\dagger(\mathbf{n})\left[\prod_{k\in\text{path}}U_k\right]\Psi(\mathbf{n}+\mathbf{R}) , \tag{3.2}$$

where the path extends from $\mathbf{n}$ to $\mathbf{n}+\mathbf{R}$ but otherwise arbitrary. Therefore, a gauge-invariant $q\bar{q}$ state in the pure gluon background can be written as

$$\Psi^\dagger(\mathbf{n})\left[\prod_{k\in\text{path}}U_k\right]\Psi(\mathbf{n}+\mathbf{R})|\psi_0\rangle|\,\rangle_F , \tag{3.3}$$

where $|\,\rangle_F$ is the fermion vacuum, and $|\psi_0\rangle$ is a pure gluon vacuum for which we choose the single-plaquette product of equation (2.3). It is clear from Eq. (3.3) that the Hilbert space of these states is infinite, so we shall assume the following simplifications [placing q at the origin and $\bar{q}$ at the site $\mathbf{n}=(n_x,n_y,n_z)$]; the paths of Eq. (3.3) are chosen to be the shortest paths connecting the origin $\mathbf{o}$ to $\mathbf{n}$, as suggested from strong-coupling perturbation, and further we will restrict $\bar{q}$ to the xy plane. With this choice for a given path containing n_x+n_y links, the dimension of the subspace is $(n_x+n_y)!/n_x!n_y!$. The heavy-quark potential is the difference between the ground-state energy with $q\bar{q}$ pair present and the vacuum energy. Let the ith state denote the various states of Eq. (3.3):

$$\begin{aligned}|i\rangle&=\Psi^\dagger(n_x,n_y)F_i\Psi(0,0)|\psi_0\rangle\\ F_i&=\prod_{k\in\text{path }i}U_k ,\end{aligned} \tag{3.4}$$

where U_k is the kth link in the path i.

Then we need to calculate $\langle i|H|j\rangle$ and $\langle i|j\rangle$. The magnetic term contribution is

$$\frac{\left\langle i\left|\sum_p (2-\mathrm{tr}U_p)\right|j\right\rangle}{\langle\psi_0|\psi_0\rangle}=2N_p\langle \mathrm{tr}(F_i^\dagger F_j)\rangle-\frac{1}{2}\frac{\partial}{\partial\lambda}\langle \mathrm{tr}(F_i^\dagger F_j)\rangle-\left\langle\sum_p \mathrm{tr}U_p\right\rangle\langle \mathrm{tr}(F_i^\dagger F_j)\rangle$$
$$=\left\langle\sum_p (2-\mathrm{tr}U_p)\right\rangle\langle \mathrm{tr}(F_i^\dagger F_j)\rangle-\frac{1}{2}\frac{\partial}{\partial\lambda}\langle \mathrm{tr}(F_i^\dagger F_j)\rangle\ , \tag{3.5}$$

where we divided by $\langle\psi_0|\psi_0\rangle$ for convenience and the expectation values of the various terms are taken with respect to $|\psi_0\rangle$. The contribution of the electric term is

$$\frac{\left\langle i\left|\sum_k\sum_a E_k^a E_k^a\right|j\right\rangle}{\langle\psi_0|\psi_0\rangle}=\frac{3}{2}\lambda\left[\frac{1}{2}\frac{\partial}{\partial\lambda}\langle \mathrm{tr}(F_i^\dagger F_j)\rangle+\left\langle\sum_p \mathrm{tr}U_p\right\rangle\langle \mathrm{tr}(F_i^\dagger F_j)\rangle\right]+\frac{3}{8}[n_x+n_y+C_{ij}(n_x,n_y)]\langle \mathrm{tr}(F_i^\dagger F_j)\rangle\ , \tag{3.6}$$

where $C_{ij}(n_x,n_y)$ is the number of common links between F_i and F_j. The derivation of Eqs. (3.5) and (3.6) is given in Appendix B. Thus

$$\frac{\langle i|aH|j\rangle}{\langle\psi_0|\psi_0\rangle}=N_p\left[\frac{3\lambda}{8\xi}-4\xi\right]P(\lambda)\langle \mathrm{tr}(F_i^\dagger F_j)\rangle+\left[\frac{3\lambda}{16\xi}-2\xi\right]\frac{\partial}{\partial\lambda}\langle \mathrm{tr}(F_i^\dagger F_j)\rangle+\frac{3}{32\xi}[n_x+n_y+C_{ij}(n_x,n_y)]\langle \mathrm{tr}(F_i^\dagger F_j)\rangle\ , \tag{3.7}$$

where the first term is just the vacuum contribution. Thus

$$V_{ij}(n_x,n_y)=+\left[\frac{3\lambda}{16\xi}-2\xi\right]\frac{\partial}{\partial\lambda}\langle \mathrm{tr}(F_i^\dagger F_j)\rangle+\frac{3}{32\xi}[n_x+n_y+C_{ij}(n_x,n_y)]\langle \mathrm{tr}(F_i^\dagger F_j)\rangle \tag{3.8}$$

are the matrix elements of the static quark potential. The states of Eq. (3.4) are not orthonormal:

$$\frac{\langle i|j\rangle}{\langle\psi_0|\psi_0\rangle}=\langle \mathrm{tr}F_i^\dagger F_j\rangle\equiv M_{ij}\ . \tag{3.9}$$

We need to diagonalize M_{ij} to find the lowest-energy eigenvalue. To do so, we use the Schmidt orthogonalization method, which gives the orthonormal set

$$|k\rangle=(SD^{-1/2})_{ki}|i\rangle\ , \tag{3.10}$$

where

$$S^\dagger MS=D\ . \tag{3.11}$$

S is a transformation which diagonalizes M, and D is the resulting diagonal matrix. Thus the matrix elements of the $q\bar{q}$ potential in this new orthonormal basis are

$$V_{kk'}=(D^{-1/2}S^\dagger)_{ki}V_{ij}(SD^{-1/2})_{jk}\ . \tag{3.12}$$

The lowest eigenvalue obtained by diagonalizing (3.12) yields an upper limit on the ground-state energy of the $q\bar{q}$ state.

In calculating matrix elements of M and V, the quantity $\langle \mathrm{tr}(F_i^\dagger F_j)\rangle$ must be evaluated for all i and j. For example, when $n_x=2$, $n_y=1$, and $C_{ij}=1$, one needs to evaluate the expectation value of the diagram shown in Fig. 6. In general, to obtain these matrix elements we need to calculate the expectation values of planar extended plaquettes (planar since $q\bar{q}$ are in the xy plane). Using the Gross-Witten trick[21] for a generalized extended plaquette,

$$\left\langle \mathrm{tr}\left[\prod_{i=1}^m U_i\right]\right\rangle=\frac{1}{2^{m-1}}\left\langle\prod_{i=1}^m(\mathrm{tr}\,U_i)\right\rangle\ , \tag{3.13}$$

the calculation of these terms reduces to calculating the expectation values of various products of the traces of elementary plaquettes, which is done using the techniques developed in Sec. II. The variational parameter λ is determined by minimizing the ground-state energy

$$a\mathcal{E}_0=\frac{1}{N_p}\frac{\langle\Psi_0|aH|\Psi_0\rangle}{\langle\Psi_0|\Psi_0\rangle}=\left[\frac{3\lambda}{8\xi}-4\xi\right]P(\lambda)+8\xi \tag{3.14}$$

which yields

$$\xi^2=\frac{3}{128}\left[\frac{P(\lambda)}{4P'(\lambda)}+4\lambda\right]\ , \tag{3.15}$$

where the $P(\lambda)$ is the expectation value of an elementary plaquette, which is also calculated using the method de-

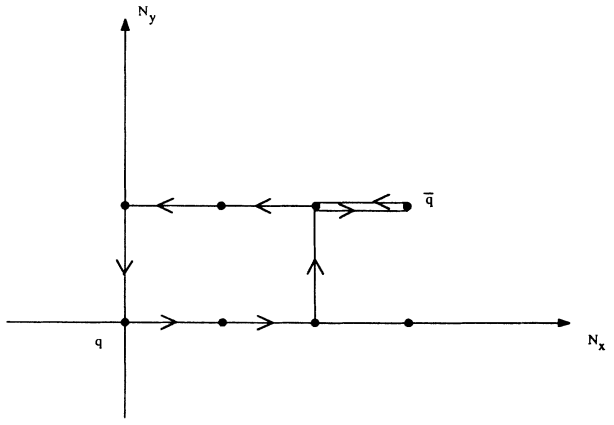

FIG. 6. $F_i^\dagger F_j$ for $n_x=2$, $n_y=1$, and $C_{ij}=1$.

scribed in Sec. II. The resulting ground-state energy density [Eq. (3.14)] is shown in Fig. 7. We have compared this result with those of Refs. 16 and 17 (Ref. 17 contains the exact calculation of the ground-state energy using a Monte Carlo guided random-walk method developed for quantum many-body problems). The agreement is excellent in both cases (in fact we reproduce the values of Ref. 16 to about 0.1% through out the range of the coupling constant, and similar deviations from the values of Ref. 17, for which at worst we differ by 2% in the last two calculated energies). In addition, we have compared our calculation with the mean-field Monte Carlo calculation,[22] and the t-expansion results.[23] It is instructive here to compare our method with the somewhat similar analysis of Ref. 22. In the mean-field method,[22] two approaches are taken to evaluate the relevant physical quantities. The first approach entails calculating expectation values of the relevant operators by directly evaluating Eq. (2.4) of this paper, using known Monte Carlo methods. Our calculated energy agrees well with the resulting energy of this approach (in fact, our energy is lower in the intermediate coupling region). In their second approach, the mean-link method, the physical states are taken to be projections on the gauge-invariant sector of a generalized functional of a product of links over the whole lattice. This projection entails the introduction of SU(2) rotations on the vertices of the lattice. The partition function is obtained from the normalization of this wave function, and the link wave function is then expanded in characters of the group. The integrals involved are thus carried out in link space, and over the vertices functions. This method differs in two aspects from the one presented in this work. First, our integration is carried out in plaquette variables (rather than links), the Jacobian of the transformation from link space to plaquette space is the (nonlocal) Bianchi identities in Eq. (2.7). Second, we have chosen the well localized vacuum of Eq. (2.3) for a trial ground state. The latter aspect is what made the Abelianization approximation of the Bianchi identities valid in the completely fixed axial-like gauge (as was shown in Sec. I, the contribution of the non-Abelianized identities are negligible; a result which is related to the choice of the vacuum). This in turn preserved the local nature of our integrals. The Bianchi identities due to this approximation are then expanded in group characters of the appropriate plaquettes; thus making the analytic solution possible. However, the mean-link approach of Ref. 22 does not utilize such approximations; this rendered the symmetry of their partition function that of a global SU(2), which produced (as expected) a phase transition in the calculated β function. In addition, because of the large number of configurations needed, the icosahedral subgroup of SU(2) was used, which, as was shown there, starts deviating from the continuous SU(2) in the weak-coupling region. The question remains however that, in our approach, if one uses a different vacuum, as possibly required in the deep weak-coupling region, whether the Abelianization approximation is still valid. We shall elaborate on this point in the discussion section. Our calculated energy agrees well with the t-expansion result of Ref. 23 in the intermediate coupling regime. However, their calculation becomes unreliable in the weak-coupling regime ($\xi \geq 0.5$) for the particular terms in the expansion they have considered; a possible cure for this problem is to include higher-order terms in the expansion, which proved to be difficult.

Using the procedure described above, we calculated the static quark potential, the results of which are shown in Fig. 8 for the separations $(n_x=1,n_y=3)$, $(n_x=2,n_y=2)$, $(n_x=2,n_y=3)$, and $(n_x=3,n_y=3)$ as a function of $\xi=1/2g^2$. From the static quark potential, we can locate the roughening point by studying the equipotential surfaces as a function of ξ. Our calculation[19] yields $\xi_R=0.26$ and the equipotential surfaces remains smooth up to $\xi=0.32$ at which point they start to distort (this is again due to the breakdown of the trial vacuum we used in the weak-coupling region). The smoothness of the equipotentials beyond the roughening transition is a result of using a nontrivial vacuum (as pointed out by Tonkin[8]), in contrast with SCE calculations. This can be seen from Eq. (3.3) where in the strong-coupling limit

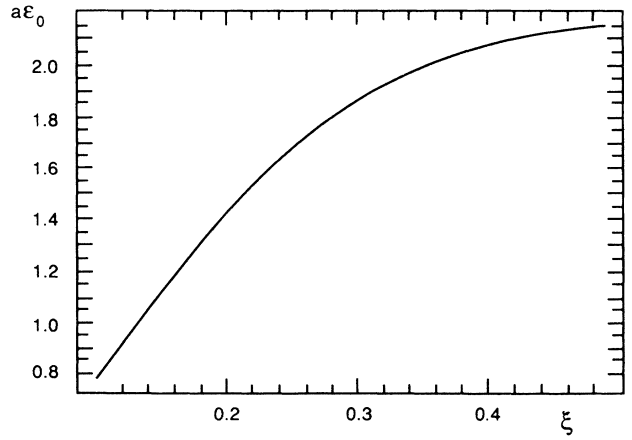

FIG. 7. The ground-state energy density as a function of $\xi=1/2g^2$.

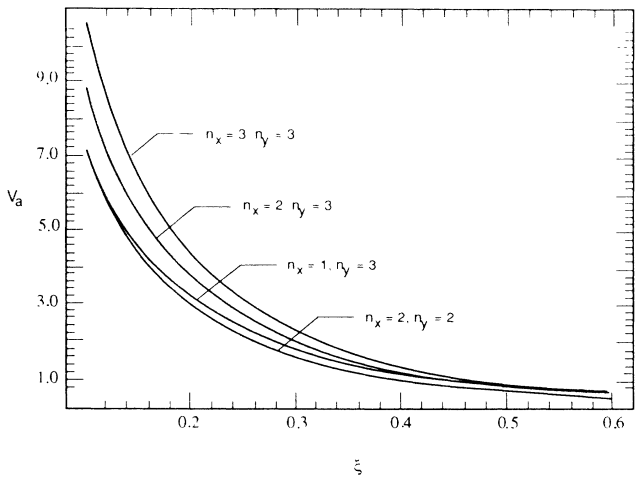

FIG. 8. The static potential for the configurations shown.

($\lambda=0$) the vacuum becomes rigid unlike the general case ($\lambda\neq 0$) where magnetic fluctuations are permitted, and gluon condensate is present (gluon loops), thus stabilizing the behavior of the potential. Our result for ξ_R is consistent with the Lagrangian Monte Carlo calculations of Ref. 24 (ξ_R in the present calculation is slightly higher than that of Ref. 24; this however can be understood if we recall that the coupling constant in the Hamiltonian formalism is slightly smaller than its counterpart in the Lagrangian formalism), but ξ_R calculated here is smaller than SCE value, in agreement with Tonkin's conclusion.

Another important quantity that can be extracted from the heavy-quark potential is the string tension, shown in Fig. 9 along with the expected scaling line. Scaling behavior is strongly suggested by the figure yielding

$$\Lambda_H = 0.009\sqrt{\sigma} \ , \tag{3.16}$$

where σ is the string tension. Using this value with the predicted string tension in the Lagrangian formalism,[25]

$$\Lambda_L = (0.0119\pm 0.0015)\sqrt{\sigma} \ , \tag{3.17}$$

we find that

$$\frac{\Lambda_H}{\Lambda_L} = 0.76\pm 0.11 \ ,$$

in accordance with $\Lambda_H/\Lambda_L = 0.84$ obtained by Hasenfratz and Hasenfratz.[26] It is interesting to see whether scaling will be faster if a more complicated vacuum is used (e.g., two plaquette correlations included). This calculation is presently underway.

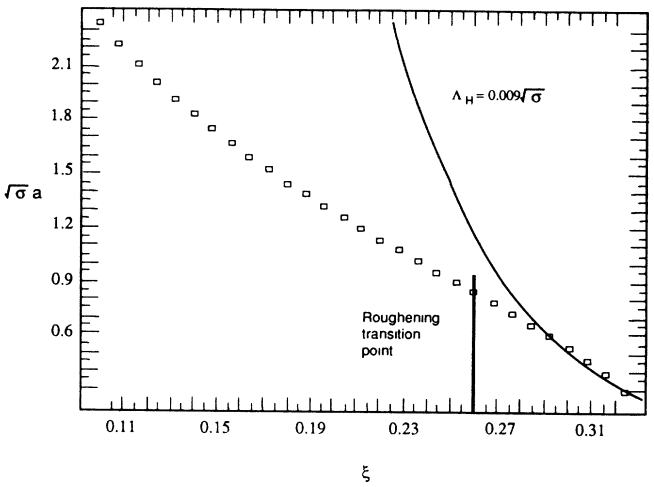

FIG. 9. The string tension as a function of the coupling constant. The solid line is the expected asymptotic scaling line.

B. The glueball mass

The results shown in Sec. III A indicate that the trial vacuum we have chosen is reasonable in the intermediate coupling region (the scaling region). In this subsection we turn to investigate the excited states, and in particular to calculate the 0^{++} glueball mass which represents the energy difference between the lowest excited state and the ground state.

Here also we shall use the single-plaquette-product for the ground-state wave functional, Eq. (2.3), and for the trial lowest excited state we use a projector including correlations up to two adjacent plaquettes. The choice of the latter stems from the fact that simple plaquette projectors were not sufficient to produce scaling of the glueball mass in recent Monte Carlo studies of SU(N) done by Chin, Long, and Robson,[18] even for $N=3$.

The excited-state projector is

$$|\psi_1\rangle = \tilde{F}|\psi_0\rangle, \quad \tilde{F} = F - \langle F\rangle \ , \tag{3.18}$$

where $\langle F\rangle$ is the expectation value of F with respect to the ground state $|\psi_0\rangle$, and

$$F = \frac{1}{\sqrt{N_p}}\left[\beta_1 \sum_p \phi_1(P) + \beta_2 \sum_{p_2} \phi_2(P_2) + \beta_3 \sum_{p_3} \phi_3(P_3)\right] , \tag{3.19}$$

where β_i are variational parameters, $\phi_1(P)$ is the trace of an elementary plaquette [Fig. 10(a)], $\phi_2(P_2)$ is the trace of an extended planar plaquette shown in Fig. 10(b), and $\phi_3(P_3)$ is the trace of the extended plaquette shown in Fig. 10(c). The expectation value of F, $\langle F\rangle$, is included in (3.18) to ensure orthogonality of $|\psi_1\rangle$ to $|\psi_0\rangle$.

The energy of the excited state is derived in Appendix B, and the result is

$$aE_1[\Psi_1] = \frac{\langle\Psi_1|aH|\Psi_1\rangle}{\langle\Psi_1|\Psi_1\rangle} = \left[\frac{3\lambda}{8\xi}\left\langle\sum_p \mathrm{tr}U_p\right\rangle + 4\xi(2-\mathrm{tr}U_p)\right] + \left[\frac{3\lambda}{8\xi} - 4\xi\right]\frac{1}{2}\frac{\partial}{\partial\lambda}\ln\langle\tilde{F}^\dagger\tilde{F}\rangle$$
$$+ \frac{1}{16\xi}\sum_k\sum_a\left[\frac{\langle[E_k^a,[E_k^a,F^\dagger]]\tilde{F}\rangle}{\langle\tilde{F}^\dagger\tilde{F}\rangle} + \frac{\langle\tilde{F}^\dagger[E_k^a,[E_k^a,F]]\rangle}{\langle\tilde{F}^\dagger\tilde{F}\rangle} - 2\frac{\langle[E_k^a,F^\dagger][E_k^a,F]\rangle}{\langle\tilde{F}^\dagger\tilde{F}\rangle}\right] , \tag{3.20}$$

which implies [since the first term in (3.20) is the ground-state energy]

$$M_g a = a(E_1 - E_0) = \left[\frac{3\lambda}{8\xi} - 4\xi\right]\frac{1}{2}\frac{\partial}{\partial\lambda}\ln\langle\tilde{F}^\dagger\tilde{F}\rangle$$
$$+ \frac{1}{16\xi}\sum_k\sum_a\left[\frac{\langle[E_k^a,[E_k^a,F^\dagger]]\tilde{F}\rangle}{\langle\tilde{F}^\dagger\tilde{F}\rangle} + \frac{\langle\tilde{F}^\dagger[E_k^a,[E_k^a,F]]\rangle}{\langle\tilde{F}^\dagger\tilde{F}\rangle} - 2\frac{\langle[E_k^a,F^\dagger][E_k^a,F]\rangle}{\langle\tilde{F}^\dagger\tilde{F}\rangle}\right] . \tag{3.21}$$

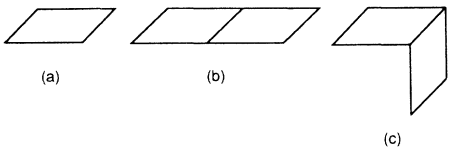

FIG. 10. The operators used in the projector F: (a) an elementary plaquette, (b) and extended planar plaquette, and (c) an extended nonplanar plaquette.

If one assumes that the ground state is exact, Eq. (3.21) reduces to

$$M_g a = \frac{1}{2}\frac{\langle [F^\dagger,[aH,F]]\rangle}{\langle \tilde{F}^\dagger \tilde{F}\rangle} = -\frac{1}{4\xi}\sum_k \sum_a \frac{\langle (E_k^a F^\dagger)(E_k^a F)\rangle}{\langle \tilde{F}^\dagger \tilde{F}\rangle} . \tag{3.22}$$

This clearly is the case in the strong-coupling region, but it may not be true in the weaker-coupling regions; therefore, we shall evaluate the glueball mass using Eqs. (3.21) and (3.22). This will be a good test for the validity of the trial vacuum chosen here.

Using Eq. (3.19), Eq. (3.21) becomes

$$M_g a\xi = \frac{1}{\sum_{i,j=1}^{3}\beta_i^* D_{ij}\beta_j}\left[\frac{1}{8}\sum_{i,j=1}^{3}\beta_i^* N_{ij}\beta_j + \frac{1}{16}\sum_{i,j=1}^{3}\beta_i^* Q_{ij}N_{ij}\beta_j + \left[\frac{3\lambda}{8}-4\xi^2\right]\times\sum_{i,j=1}^{3}\beta_i^*\left[\frac{1}{2}\frac{\partial}{\partial\lambda}D_{ij}\right]\beta_j\right] \tag{3.23}$$

and Eq. (3.22) becomes

$$M_g a\xi = \frac{1}{4}\frac{\sum_{i,j=1}^{3}\beta_i^* N_{ij}\beta_j}{\sum_{i,j=1}^{3}\beta_i^* D_{ij}\beta_j} , \tag{3.24}$$

where

$$N_{ij} = -(1+\delta_{i,2}+3\delta_{i,3})\times\left\langle \sum_k\sum_a [E_k^a\phi_i^*(0)]\left[E_k^a\sum_p\phi_j(p)\right]\right\rangle , \tag{3.25}$$

$$D_{ij} = (1+\delta_{i,2}+3\delta_{i,3})\times\left[\left\langle\phi_i^*(0)\sum_p\phi_j(p)\right\rangle - \langle\phi_i^*(0)\rangle\left\langle\sum_p\phi_j(p)\right\rangle\right] , \tag{3.26}$$

$$Q_{ij} = \begin{bmatrix} 6 & \frac{15}{2} & \frac{15}{2} \\ \frac{15}{2} & 9 & 9 \\ \frac{15}{2} & 9 & 9 \end{bmatrix} , \tag{3.27}$$

$\phi_i(0)$ denotes the trace of the ith-type plaquette at a fixed position and the overall factor $(1+\delta_{i2}+3\delta_{i3})$ results from counting the number of the different types of plaquettes on a lattice whose total number of plaquettes is N_p. The minimization condition, $(\partial/\partial\beta_i)(Mga\xi)=0$, yields

$$\det\left|\tfrac{1}{8}N+\tfrac{1}{16}QD+\left[\frac{3\lambda}{8}-4\xi^2\right]\frac{1}{2}\frac{\partial}{\partial\lambda}D-(M_g a\xi)D\right|=0 \tag{3.28}$$

for Eq. (3.23) and

$$\det\left|\tfrac{1}{4}N-(\xi M_g a)D\right|=0 \tag{3.29}$$

for Eq. (3.24), the solution of which give the glueball mass.

Since the electric field operator acts on common links, the only contributions to the matrix elements of N comes from connected diagrams, which include adjacent diagrams with a common link and overlapped diagrams. Consider two adjacent plaquettes U_{p_1} and U_{p_2} which have a common link. Then

$$\left\langle\sum_k\sum_a (E_k^a \mathrm{tr}\tilde{U}_{p_1})(E_k^a\mathrm{tr}\tilde{U}_{p_2})\right\rangle = \left\langle\sum_a \mathrm{tr}\left[\frac{\tau^a}{2}\tilde{U}_{p_1}\right]\mathrm{tr}\left[\frac{\tau^a}{2}\tilde{U}_{p_2}\right]\right\rangle = \tfrac{1}{4}[2\langle\mathrm{tr}(\tilde{U}_{p_1}\tilde{U}_{p_2})\rangle - \langle\mathrm{tr}\tilde{U}_{p_1}\mathrm{tr}\tilde{U}_{p_2}\rangle] , \tag{3.30}$$

where we used

$$\sum_a\left[\frac{\tau^a}{2}\right]_{ij}\left[\frac{\tau^a}{2}\right]_{km} = \tfrac{1}{4}(2\delta_{i,m}\delta_{j,k}-\delta_{i,j}\delta_{k,m})$$

in the second equality in (3.30). However, using the Gross-Witten trick,[21] Eq. (3.13), Eq. (3.30) vanishes to a very good approximation (the reason why it does not vanish identically is the existence of correlations due to the Bianchi identities, which nonetheless we verified to be negligible), thus the major contribution to N comes from overlapped diagrams shown in Figs. 11(a)–11(d) with their respective multiplicities.

From Eq. (3.26) it is clear that the matrix elements D_{ij} signify the correlation effects. In the case where either i or j equals 1 (i.e., when an elementary plaquette is involved), we have

$$D_{i1} = (1+\delta_{i,2}+3\delta_{i,3})\left[\frac{1}{2}\frac{\partial}{\partial\lambda}\langle\phi_i(0)\rangle\right] . \tag{3.31}$$

When neither i nor j is equal to 1, the situation is a little more complicated. Notice that we have three types of diagrams; disconnected (no common link), connected, and overlapped. The dominant contribution to correlations obviously comes from the overlapped diagrams. To manage the calculation, we introduce the following approximation: to first order, approximate the correlations between two extended plaquettes by the correlation between an elementary plaquette and one extended plaquette. For example, this gives, for D_{22},

$$D_{22}=2\left[\left\langle\phi_2(0)\sum_p\phi_2(p)\right\rangle-\langle\phi_2(0)\rangle\left\langle\sum_p\phi_2(p)\right\rangle\right]$$
$$\approx 4\langle\phi_1(0)\rangle\left[\left\langle\phi_2(0)\sum_p\phi_1(p)\right\rangle-\langle\phi_2(0)\rangle\left\langle\sum_p\phi_1(p)\right\rangle\right]$$
$$\approx 4\langle\phi_1(0)\rangle\left[\frac{1}{2}\frac{\partial}{\partial\lambda}\langle\phi_2(0)\rangle\right]\equiv D_{22}^{(0)}\ ,$$

where we have used the Gross-Witten trick to get the second equality.

In general we therefore have

$$D_{ij}^{(0)}=\tfrac{1}{2}(1+\delta_{i,2}+3\delta_{i,3})(1+\delta_{j,2}+3\delta_{j,3})\times\langle\phi_1(0)\rangle\left[\frac{1}{2}\frac{\partial}{\partial\lambda}\langle\phi_i(0)\rangle+\frac{1}{2}\frac{\partial}{\partial\lambda}\langle\phi_j(0)\rangle\right]$$
for $i\neq 1$ and $j\neq 1$. (3.32)

Since the overlapped diagrams are the dominant contri-

Matrix Element	Type of Diagrams	Number of Diagrams
N_{11}	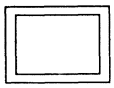	1
N_{12}	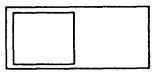	4
N_{13}	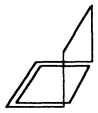	8

(a)

Type of Diagrams	Number of Diagrams
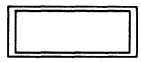	2
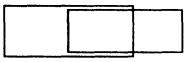	4
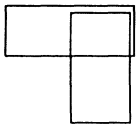	8

(b)

Type of Diagrams	Number of Diagrams
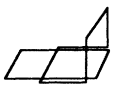	4
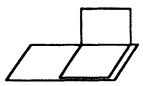	16
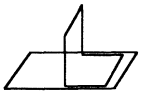	8

(c)

Type of Diagrams	Number of Diagrams
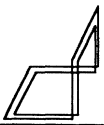	4
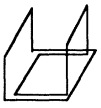	8
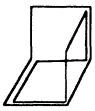	16
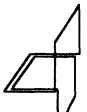	8
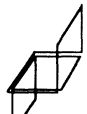	8
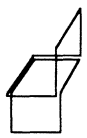	16

(d)

FIG. 11. The overlapped diagrams contributing to (a) N_{i1}, $i=1,2,3$; (b) N_{22}; (c) N_{23} and (d) N_{33}.

butors to D, we calculate those exactly and add the difference between their contribution and the approximation above to Eq. (3.32) (to a large part, the correlations of the disconnected and connected diagrams come from the Bianchi identities; this is clearly the case for the disconnected diagrams), thus

$$D_{ij} \approx D_{ij}^{(0)} + D_{ij}^{(1)} \quad \text{for } i \neq 1 \text{ and } j \neq 1 , \tag{3.33}$$

where $D_{ij}^{(1)}$ for $i \neq 1$ and $j \neq 1$ are displayed in Fig. 12.

The expectation values of the different plaquettes in N and D can now be calculated using the formulas derived in Sec. II, and in turn the matrices N_{ij} and D_{ij} can now be substituted in Eqs. (3.28) and (3.29) to yield the different estimates of the glueball mass. Figure 13 displays our results for the glueball mass obtained by solving Eqs. (3.28) and (3.29) (I and II, respectively) along with the asymptotic scaling lines (shown also in the inset is the approximate glueball mass in units of Λ_H for both curves). Both curves show an obvious tendency for scaling, especially the solution of Eq. (3.28) (notice that in both cases, the curves start diverging at $\xi \approx 0.3$, indicating the breakdown of our approximation.) They both coincide in the strong-coupling region, which agrees with the fact that the vacuum chosen is exact in that regime but scaling is faster for curve I, implying that one should not assume that the ground state given by Eq. (2.3) is exact. The approximate glueball mass obtained for curve I is in good agreement with present predictions. To confirm this, we have calculated the ratio $R = Mg/\sqrt{\sigma}$, the result of which is shown in Fig. 14. Our calculated R

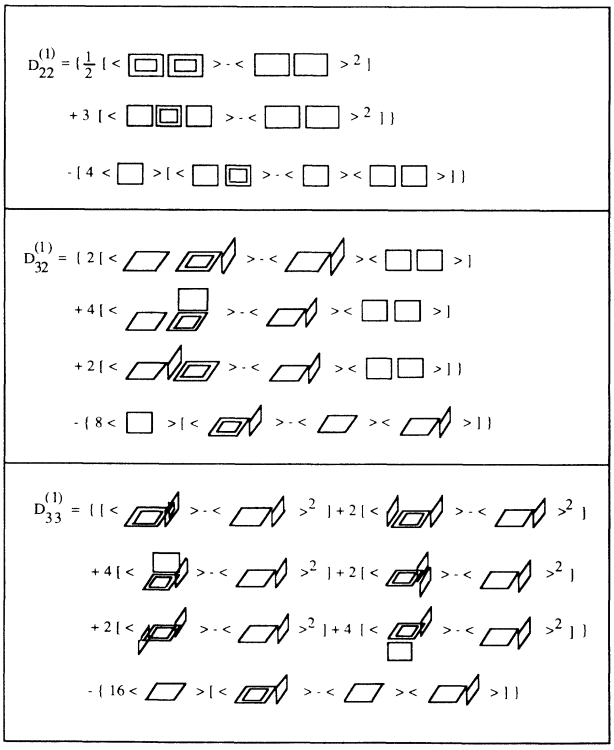

FIG. 12. The matrix elements $D_{ij}^{(1)}$ for $i \neq 1$ and $j \neq 1$.

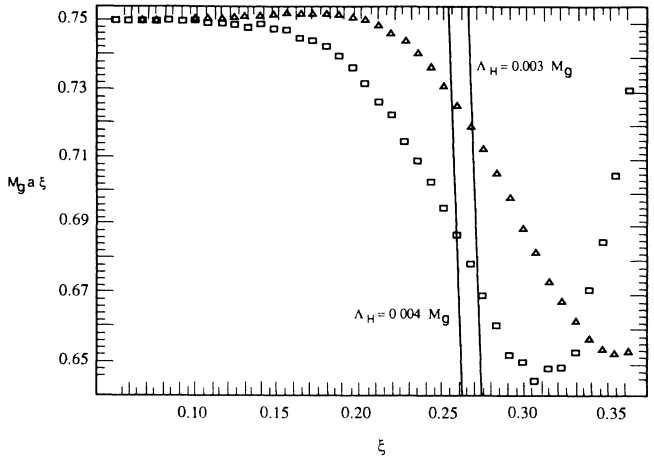

FIG. 13. The glueball mass. The squares are the result of Eq. (3.29), and the triangles are those of Eq. (3.30). The solid lines are the expected asymptotic scaling lines.

displays quite well the expected generic behavior described by Chin and Karliner.[28] In particular, R starts from extreme strong coupling with no scaling, then it exhibits constancy over a reasonable range of the coupling constant at weaker coupling, resulting in the value $R = 2.86$. At weak couplings the ratio R begins to diverge due to the fact that our single-plaquette vacuum is not adequate in this region. [Notice that this is a general feature of many SU(N) calculations of $R = Mg/\sqrt{\sigma}$, as indicated by Ref. 28 which displayed various results of this ratio starting at $\xi \equiv 1/Ng^2 = 0.1$. At $\xi = 0.4$, R for SU(5) and SU(6) starts diverging with an identical behavior to that displayed by our calculations. For SU(3), this divergence starts at $\xi \approx 0.3$. Near this value the ratio R in the present method starts diverging, indicating the reasonability of our approximation, since at smaller N one would expect the need for higher correlations.[27]] The value $R = 2.86$ obtained here agrees well with $R = 2.8 \pm 0.3$ calculated using Euclidean Monte Carlo simulation of Fukugita *et al.*[29] Moreover, this is in fair

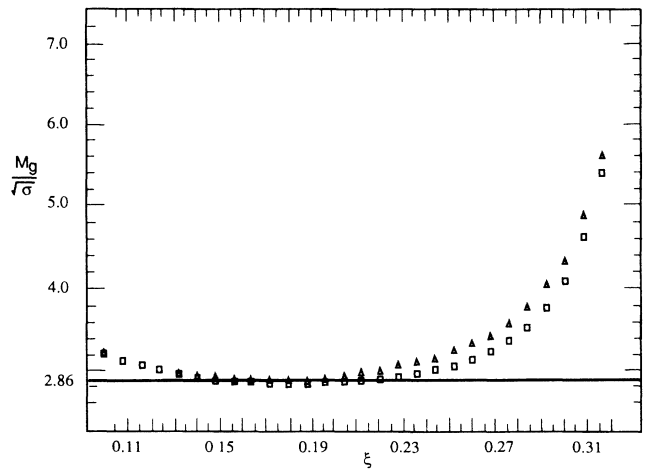

FIG. 14. The ratio of the glueball mass [squares from Eq. (3.29) and triangles from (3.30)] to the string tension

agreement with the value calculated in Ref. 23 using the t-expansion method ($R=3.5\pm0.2$) and the value obtained by DeGrand and Peterson[30] ($R=3.4\pm0.3$). The difference between our result and the latter two can be attributed to the possibility that a more correlated vacuum is needed in the intermediate coupling regime. We will elaborate on this further in the discussion and conclusion section. Using $R=2.86$ implies

$$Mg=2.86\sqrt{\sigma}\ ,$$

in reasonable agreement with the recent estimate of Berg and Billoire[31] $\sqrt{\sigma}=(0.315\pm0.030)M_g$.

IV. DISCUSSION AND CONCLUSION

We have developed an analytic variational method for calculating the various physical quantities in Hamiltonian lattice gauge theory, which is based on Batrouni's mean-plaquette approximation[15] and Robson's plaquette space integration.[11]

In the course of developing this approach, we have shown that the effects of the non-Abelianized Bianchi identities are negligible and that the convergence of the Bianchi identities's character expansion is very fast (the B curves converged always at $j=1$). We have later, in Sec. III, applied this method to the calculation of the off-axis heavy-quark potential. Several important results were obtained (see Ref. 19 for details and discussions of these results): the roughening transition point was calculated to be $\xi_R=0.26$; this value lies in a stronger-coupling region compared to that obtained by strong-coupling techniques and close to the Monte Carlo estimates of Ref. 24. In addition, the equipotential surfaces obtained remained smooth up to $\xi=0.32$ due to the use of the nontrivial vacuum, Eq. (2.3). Finally, scaling for the string tension was observed, yielding $\Lambda_H=0.009\sqrt{\sigma}$, which was used to calculate the ratio Λ_H/Λ_L, the value of which agrees well with that predicted by Hasenfratz and Hasenfratz.[26]

Next, we calculated the glueball mass with and without the exact ground-state assumption. We have shown there that this assumption is questionable in the intermediate coupling region; the glueball mass curves showed a clear tendency to scaling, and the ratio $R=Mg/\sqrt{\sigma}$ displayed a reasonable scaling behavior, which in return gave $Mg=2.86\sqrt{\sigma}$. The ratio R is in good agreement with previous calculations.[23,29,31] In particular, our R value is in a satisfactory agreement with the value obtained in Ref. 30, and with the t-expansion calculations,[23] unfortunately however, the series expansion in the latter for the string tension and the glueball mass separately do not have enough terms to reliably calculate these quantities, and thus we could not compare our corresponding results.

These are by no means our final results, and many different aspects of this program need to be investigated, in particular questions related to scaling of the glueball mass. It is clear from Fig. 13 that the mass gap scaling is slow. This had the effect of moving the scaling window of the ratio R toward the strong-coupling region as seen from Fig. 14. Calculations in $2+1$ dimensions[7,8] indicate that the single-plaquette product vacuum [Eq. (2.35)] may not be adequate in the intermediate coupling region, thus higher correlations may be needed to overcome the scaling problem.[22] The vacuum chosen in the present method although variational—hence permitting magnetic fluctuations—has the structure of the strong-coupling vacuum; this could be responsible for the slow scaling of the mass gap and the relatively strong scaling of the ratio R. As pointed out in the Introduction, variational methods have their own intrinsic errors, e.g., they provide only bounds on the various quantities under consideration. An alternative to modifying the ground state is to modify the first excited state to include more correlations for the calculation of the glueball mass, such as done in Ref. 32, by including correlations up to four elementary plaquettes. To clearly settle the issue, one has to perform the required calculations.

Presently, we are in the process of calculating the glueball mass using a variational vacuum which includes correlations up to two elementary plaquettes, utilizing a perturbative expansion similar to that of Arisue, Kato, and Fujiwaru[7] (solving the problem nonperturbatively turned out to be very difficult). In addition, an important question to be addressed is whether the Abelianization approximation is valid for this modified vacuum. There is strong evidence that this is the case (as mentioned in Sec. I, the expectation value of extended plaquettes using the method presented here are in accord with our Monte Carlo results; also as shown in Ref. 15, this transformation can be done exactly for a $2\times\infty$ lattice, and approximately for a large region of arbitrary lattices); however, further considerations are needed. Although we have observed scaling of the string tension using the vacuum Eq. (2.3), it will be interesting to see the effect of this new vacuum described above on its scaling behavior and on the value of $\sqrt{\sigma}$. Another interesting effect to be sought is the value of the roughening point; especially whether this "improved" vacuum pushes ξ_R closer to the value estimated by SCE or further away.

ACKNOWLEDGMENTS

We are very grateful to D. Robson for many discussions during the course of this work. We also would like to thank R. L. Coldwell for his help and suggestions in several numerical problems.

APPENDIX A

1. The evaluation of Eq. (2.14)

To evaluate the right hand side of Eq. (2.14), notice that apart from the measure and the factor $\exp(2\lambda\mathrm{tr}U_{p_m})$, the numerator and the denominator are powers of the different characters. To avoid confusion, we write (2.14) in the form

$$\langle \mathrm{tr}U_p\rangle=\frac{\sum_{j_1}\sum_{j_2}N_{j_1j_2}}{\sum_{j_1}\sum_{j_2}D_{j_1j_2}}\ ,$$

where

$$N_{j_1 j_2}=\int \left[\prod_{i=1}^{11} dU_{p_i}\right]\left[\frac{1}{(2j_1+1)^4}\frac{1}{(2j_2+1)^4}\chi_{j_1}(U_{p_1})\chi_{j_2}(U_{p_1})\left[\prod_{k=2}^{6}\chi_{j_1}(U_{p_k})\right]\left[\prod_{n=7}^{11}\chi_{j_2}(U_{p_n})\right]\right]$$
$$\times(\mathrm{tr}U_{p_1})\prod_{m=1}^{11}\exp(2\lambda\,\mathrm{tr}U_{p_m})$$

and

$$D_{j_1 j_2}=\int \left[\prod_{i=1}^{11} dU_{p_i}\right]\left[\frac{1}{(2j_1+1)^4}\frac{1}{(2j_2+1)^4}\chi_{j_1}(U_{p_1})\chi_{j_2}(U_{p_1})\left[\prod_{k=2}^{6}\chi_{j_1}(U_{p_k})\right]\left[\prod_{n=7}^{11}\chi_{j_2}(U_{p_n})\right]\right]\prod_{m=1}^{11}\exp(2\lambda\,\mathrm{tr}U_{p_m})\,. \tag{A1}$$

Multiplying this by

$$1=\frac{\int\left[\prod_{i=1}^{11} dU_{p_i}\right]\prod_{m=1}^{11}\exp(2\lambda\,\mathrm{tr}U_{p_m})}{\int\left[\prod_{i=1}^{11} dU_{p_i}\right]\prod_{m=1}^{11}\exp(2\lambda\,\mathrm{tr}U_{p_m})}$$

we obtain

$$\langle \mathrm{tr}U_p\rangle=\frac{\sum_{j_1}\sum_{j_2}N'_{j_1 j}}{\sum_{j_1}\sum_{j_2}D'_{j_1 j_2}}\,,$$

where

$$N'_{j_1 j_2}=N_{j_1 j_2}\Big/\int\left[\prod_{i=1}^{11} dU_{p_i}\right]\prod_{m=1}^{11}\exp(2\lambda\,\mathrm{tr}U_{p_m})$$

and

$$D'_{j_1 j_2}=D_{j_1 j_2}\Big/\int\left[\prod_{i=1}^{11} dU_{p_i}\right]\prod_{m=1}^{11}\exp(2\lambda\,\mathrm{tr}U_{p_m})\,. \tag{A2}$$

Then it is clear that (A1) reduces to calculating (2+1)-dimensional expectation values of the different characters (and their powers). For example (defining $P\equiv\mathrm{tr}Up$),

$$N'_{00}=N_{00}\Big/\int\left[\prod_{i=1}^{11} dU_{p_i}\right]\prod_{m=1}^{11}\exp(2\lambda\,\mathrm{tr}U_{p_m})$$
$$=\frac{\int dU_p\,\mathrm{tr}U_p\exp(2\lambda\,\mathrm{tr}U_p)}{\int dU_p\exp(2\lambda\,\mathrm{tr}U_p)}=\langle P\rangle'\,,$$

where primes on the expectation value denote the corresponding quantities in 2+1 dimensions; this integral was given in Eq. (2.15).

Similarly,

$$N'_{01/2}=N_{01/2}\Big/\int\left[\prod_{i=1}^{11} dU_{p_i}\right]\prod_{m=1}^{11}\exp(2\lambda\,\mathrm{tr}U_{p_m})$$
$$=\tfrac{1}{16}\langle p\rangle'^6\langle p^2\rangle'\,.$$

In the same way we can reduce the different terms of N' and D' in terms of various (2+1)-dimensional matrix elements of the different powers of the given characters. Two points remain to be taken care of to complete the evaluation of (2.14). First, when we have $j\geq 1$ characters, these can be rewritten in terms of $j=\frac{1}{2}$ characters using the recursion formulas of Eq. (2.10c). The second point is that the expectation values of the different powers of P can be obtained in terms of the expectation value of P. To see this, notice that

$$\frac{\partial}{\partial 2\lambda}\langle P'\rangle=\left[\int dU_p\,\mathrm{tr}U_p\,\mathrm{tr}U_p\exp(2\lambda\,\mathrm{tr}U_p)\int dU_p\exp(2\lambda\,\mathrm{tr}U_p)\right.$$
$$\left.-\left[\int dU_p\,\mathrm{tr}U_p\exp(2\lambda\,\mathrm{tr}U_p)\right]^2\right]\Big/\left[\int dU_p(\mathrm{tr}U_p)\exp(2\lambda\,\mathrm{tr}U_p)\right]^2=\langle P^2\rangle'-\langle P\rangle'\,.$$

The derivations of $\langle P\rangle'$ can be obtained from known recursion formulas of the modified Bessel functions.[33] Similarly, the expectation values of higher powers of P can be obtained. Using the above, one can straightforwardly (with a bit of algebra) evaluate Eq. (2.14). The result of this calculation for the upper limit $j_1=j_2=1$ is

$$N_{1/2}\equiv N_{1/2\,0}+N_{0\,1/2}+N_{12\,1/2}=\tfrac{1}{8}a^4b+\tfrac{1}{256}a^9c\,,$$
$$N_1=N_{10}+N_{01}+N_{11/2}+N_{121}+N_{11}$$
$$=\frac{2}{81}\frac{1}{a}(c-a)(b-1)^5+\tfrac{1}{648}(d-b)a^4(b-1)^5$$
$$+\frac{1}{6561}\frac{1}{a}(b-1)^{10}(e-2c+a)\,,$$

$$D_{1/2}\equiv D_{120}+D_{01/2}+D_{1/2\,1/2}=\tfrac{1}{8}a^6+\tfrac{1}{256}a^{10}b\,,$$

$$D_1\equiv D_{10}+D_{01}+D_{11/2}+D_{1/2}+D_{11}$$
$$=\tfrac{2}{81}(b-1)^6+\tfrac{1}{648}a^5(b-1)^5(c-a)$$
$$+\frac{1}{6561}\frac{1}{a}(e-2c+a)(b-1)^{10}\,.$$

If both Bianchi identities are truncated at $j=\frac{1}{2}$, then $N=N_{1/2}$, and $D=D_{1/2}$.

If both Bianchi identities are truncated at $j=1$, then $N=N_{1/2}+N_1$, and $D=D_{1/2}+D_1$. Here

$$\langle \mathrm{tr}U_p\rangle_{3D}\equiv\langle \mathrm{tr}U_p\rangle_{2D}\frac{1+N}{1+D},\quad B\equiv\frac{1+N}{1+D}-1\ ,$$

$$a\equiv\langle \mathrm{tr}U_p\rangle_{2D},\quad b\equiv\langle \mathrm{tr}^2U_p\rangle_{2D},\quad c\equiv\langle \mathrm{tr}^3U_p\rangle_{2D}\ ,$$

$$d\equiv\langle \mathrm{tr}^4U_p\rangle_{2D},\quad e\equiv\langle \mathrm{tr}^5U_p\rangle_{2D}\ .$$

2. The derivation of Eqs. (2.17) and (2.18)

For two Bianchi identities, we substitute, in Eq. (2.14),

$$\chi_j(U_p)=U_{2j}(\tfrac{1}{2}\mathrm{tr}U_p)\rightarrow U_{2j}(\tfrac{1}{2}\langle \mathrm{tr}U_p\rangle)$$

for each of the surface plaquettes which gives

$$\langle \mathrm{tr}U_p\rangle=\int dU_{p_1}\sum_{j_1}\sum_{j_2}\frac{1}{(2j_1+1)^4}\frac{1}{(2j_2+1)^4}U^5_{2j_1}(\tfrac{1}{2}\langle \mathrm{tr}U_p\rangle)U_{2j_2}(\tfrac{1}{2}\langle \mathrm{tr}U_{p_1}\rangle)$$
$$\times\chi_j(U_{p_1})\exp(2\lambda\,\mathrm{tr}U_{p_1})\Big/\int dU_{p_1}\sum_{j,}\sum_{j,}\frac{1}{(2j_1+1)^4}\frac{1}{(2j_2+1)^4}U^5_{2j,}(\tfrac{1}{2}\langle \mathrm{tr}U_p\rangle)U_{2j,}(\tfrac{1}{2}\langle \mathrm{tr}U_{p_1}\rangle)\ .$$

Using Eqs. (2.10b) and (2.10c), the integration over dU_p can be done easily which yield Eq. (2.17). In exactly the same manner, with a little more algebra, Eq. (2.18) can be obtained.

APPENDIX B

1. Derivation of Eq. (3.6)

The matrix elements of the electric term in the Hamiltonian are

$$\left\langle i\left|\sum_k\sum_a E^a_kE^a_k\right|j\right\rangle=\int\left[\prod_l dU_l\right]\left[\exp\left[\frac{S}{2}\right](E^a_kE^a_k)\exp\left[\frac{S}{2}\right]\right]$$
$$=-\int\left[\prod_l dU_l\right]\left\{\left[E^a_k\exp\left[\frac{S}{2}\right]\right]\left[E^a_k\exp\left[\frac{S}{2}\right]\right]F^\dagger_jF_i+\exp\left[\frac{S}{2}\right](E^a_kF^\dagger_j)F_i\left[E^a_k\exp\left[\frac{S}{2}\right]\right]\right.$$
$$\left.+\left[E^a_k\exp\left[\frac{S}{2}\right]\right]F^\dagger_j(E^a_kF_i)\exp\left[\frac{S}{2}\right]+\exp\left[\frac{S}{2}\right](E^a_kF^\dagger_j)(E^a_kF_i)\exp\left[\frac{S}{2}\right]\right\},\tag{B1}$$

where

$$|i\rangle=\Psi^\dagger(n_x,n_y)F_i\Psi(0,0)|\psi_0\rangle$$

and, on the right-hand side, summation is implied for repeated indices. In Eq. (B1) the second equality is obtained using integration by parts and we have used

$$\langle U_p|\psi_0\rangle=\exp(S/2),\quad S\equiv2\lambda\xi_p\mathrm{tr}U_p\ .$$

For the first term we have

$$-\int\left[\prod_l dU_l\right]\left\{\left[E^a_k\exp\left[\frac{S}{2}\right]\right]\left[E^a_k\exp\left[\frac{S}{2}\right]\right]F^\dagger_jF_i\right\}=-\langle\psi_0|(E^a_k\ln\psi_0)(E^a_k\ln\psi_0)F^\dagger_jF_i|\psi_0\rangle=\tfrac{1}{2}\langle\psi_0|(E^a_kE^a_k\ln\psi_0)F^\dagger_jF_i|\psi_0\rangle$$
$$+\frac{1}{2}\int\left[\prod_l dU_l\right]\exp\left[\frac{S}{2}\right](E^a_kF^\dagger_j)F_i\left[E^a_k\exp\left[\frac{S}{2}\right]\right]$$
$$+\frac{1}{2}\int\left[\prod_l dU_l\right]\exp\left[\frac{S}{2}\right]F^\dagger_j(E^a_kF_i)\left[E^a_k\exp\left[\frac{S}{2}\right]\right]\tag{B2}$$

which gives, upon substitution in (B1),

$$\langle\psi_0|F_j^\dagger E_k^a E_k^a F_i|\psi_0\rangle=\tfrac{1}{4}\langle\psi_0|([E_k^a,[E_k^a,S]])F_j^\dagger F_i|\psi_0\rangle$$
$$-\frac{1}{2}\int\left[\prod_l dU_l\right]\exp\left[\frac{S}{2}\right](E_k^a F_j^\dagger)F_i\left[E_k^a\exp\left[\frac{S}{2}\right]\right]$$
$$-\frac{1}{2}\int\left[\prod_l dU_l\right]\exp\left[\frac{S}{2}\right]F_j^\dagger(E_k^a F_i)\left[E_k^a\exp\left[\frac{S}{2}\right]\right]$$
$$-\int\left[\prod_l dU_l\right]\exp\left[\frac{S}{2}\right](E_k^a F_j^\dagger)(E_k^a F_i)\exp\left[\frac{S}{2}\right]. \tag{B3}$$

Notice that, using integration by parts,

$$\int\left[\prod_l du_l\right]\exp\left[\frac{S}{2}\right](E_k^a F_j^\dagger)F_i\left[E_k^a\exp\left[\frac{S}{2}\right]\right]$$
$$=-\frac{1}{2}\int\left[\prod_l du_l\right]\exp\left[\frac{S}{2}\right](E_k^a E_k^a F_j^\dagger)F_i\exp\left[\frac{S}{2}\right]-\frac{1}{2}\int\left[\prod_l dU_l\right]\exp\left[\frac{S}{2}\right](E_k^a F_j^\dagger)(E_k^a F_i)\exp\left[\frac{S}{2}\right]. \tag{B4}$$

The same procedure can be applied for the third term in Eq. (B3) which yields

$$\int\left[\prod_l dU_l\right]\exp\left[\frac{S}{2}\right]F_j^\dagger(E_k^a F_i)\left[E_k^a\exp\left[\frac{S}{2}\right]\right]$$
$$=-\frac{1}{2}\int\left[\prod_l dU_l\right]\exp\left[\frac{S}{2}\right]F_j^\dagger(E_k^a E_k^a F_i)\exp\left[\frac{S}{2}\right]-\tfrac{1}{2}\int\left[\prod_l dU_l\right]\exp\left[\frac{S}{2}\right](E_k^a F_j^\dagger)(E_k^a F_i)\exp\left[\frac{S}{2}\right]. \tag{B5}$$

Substituting Eqs. (B4) and (B5) in Eq. (B3) finally gives

$$\langle\psi_0|F_j^\dagger E_k^a E_k^a F_i|\psi_0\rangle=\tfrac{1}{4}\langle\psi_0|([E_k^a,[E_k^a,S]])F_j^\dagger F_i|\psi_0\rangle+\tfrac{1}{4}\langle\psi_0|F_j^\dagger[E_k^a,[E_k^a,F_i]]|\psi_0\rangle$$
$$+\tfrac{1}{4}\langle\psi_0|[E_k^a,[E_k^a,F_j^\dagger]]F_i|\psi_0\rangle-\tfrac{1}{2}\langle\psi_0|[E_k^a,F_j^\dagger][E_k^a,F_i]|\psi_0\rangle. \tag{B6}$$

It is then straightforward to obtain Eq. (3.6) by working out each term in Eq. (B6) explicitly.

2. Derivation of Eq. (3.20)

The energy of the first excited state is

$$aE_1\equiv\frac{\langle\psi_1|aH|\psi_1\rangle}{\langle\psi_1|\psi_1\rangle}=\frac{\langle\psi_1|aH|\psi_1\rangle/\langle\psi_0|\psi_0\rangle}{\langle\psi_1|\psi_1\rangle/\langle\psi_0|\psi_0\rangle}, \tag{B7}$$

where

$$|\psi_1\rangle\equiv\tilde{F}|\psi_0\rangle=(F-\langle F\rangle)|\psi_0\rangle \tag{B8}$$

and

$$\frac{\langle\psi_1|\psi_1\rangle}{\langle\psi_0|\psi_0\rangle}=\langle\tilde{F}^\dagger\tilde{F}\rangle. \tag{B9}$$

Using Eq. (B6), it is straightforward to obtain

$$\frac{1}{4\xi}\frac{\left\langle\psi_1\left|\sum_k\sum_a E_k^a E_k^a\right|\psi_1\right\rangle}{\langle\psi_1|\psi_1\rangle}=\frac{3\lambda}{8\xi}\left[\left\langle\sum_p\mathrm{tr}U_p\right\rangle=\frac{1}{2}\frac{\partial}{\partial\lambda}\ln\langle\tilde{F}^\dagger\tilde{F}\rangle\right]$$
$$+\frac{1}{16\xi}\frac{1}{\langle\tilde{F}^\dagger\tilde{F}\rangle}\sum_k\sum_a(\langle[E_k^a,[E_k^a,F^\dagger]]\tilde{F}\rangle+\langle\tilde{F}^\dagger[E_k^a,[E_k^a,F]]\rangle-2\langle[E_k^a,F^\dagger][E_k^a,F]\rangle). \tag{B10}$$

Finally, the contribution of the magnetic term is

$$4\xi\frac{\left\langle\psi_1\left|\sum_p(2-\mathrm{tr}U_p)\right|\psi_1\right\rangle}{\langle\psi_1|\psi_1\rangle}=4\xi\left[\left\langle\sum_p(2-\mathrm{tr}U_p)\right\rangle-\frac{1}{2}\frac{\partial}{\partial\lambda}\ln\langle\tilde{F}^\dagger\tilde{F}\rangle\right]. \tag{B11}$$

*Present address: Department of Physics, Chung-Yuan Christian University Chung Li, Taiwan 32023, Republic of China.
†Present address: Space Research Institute, Florida Institute of Technology, Melbourne, FL 32901.

[1]H. D. Politzer, Phys. Rev. Lett. **30**, 1346 (1973); D. Gross and F. Wilczek, *ibid.* **30**, 1343 (1973); Phys. Rev. D **8**, 3633 (1973); H. Georgi and H. Politzer, *ibid.* **9**, 416 (1973).
[2]S. Weinberg, Phys. Rev. Lett. **31**, 494 (1973).
[3]K. G. Wilson, Phys. Rev. D **10**, 2445 (1974).
[4]M. Creutz, Phys. Rev. Lett. **43**, 533 (1978); **45**, 313 (1980); Phys. Rev. D **21**, 2308 (1980); G. Bhanot and C. Rebbi, Nucl. Phys. **B180**, 469 (1981); E. V. E. Kovacs, D. K. Sinclair, and J. B. Kogut, Phys. Rev. Lett. **58**, 751 (1987).
[5]L. H. Karsten and J. Smit, Nucl. Phys. **B183**, 103 (1981); J. B. Kogut, Rev. Mod. Phys. **55**, 775 (1983), and references therein.
[6]J. Kogut, D. K. Sinclair, and L. Susskind, Nucl. Phys. **B114**, 199 (1976); D. R. T. Jones, R. D. Kenway, J. B. Kogut, and D. K. Sinclair, *ibid.* **B158**, 102 (1979); J. Kogut, R. P. Pearson, and J. Shigemitsu, Phys. Lett. **98B**, 63 (1981).
[7]H. Arisue, M. Kato, and T. Fujiwaru, Prog. Theor. Phys. **70**, 229 (1983); A. Duncan and R. Roskies, Phys. Rev. D **31**, 364 (1985).
[8]S. P. Tonkin, Nucl. Phys. **B292**, 573 (1987).
[9]M. C. Huang, Ph.D. thesis, University of Florida, 1988.
[10]G. G. Batrouni, Nucl. Phys. **B208**, 12 (1982).
[11]D. Robson, Proceedings of the Workshop on Hamiltonian Lattice Gauge Theory Monte Carlo Methods, Tallahassee, Florida, 1987 (unpublished).
[12]J. Kogut and L. Susskind, Phys. Rev. D **11**, 395 (1975).
[13]R. P. Feynman, Nucl. Phys. **B188**, 579 (1981); J. P. Greensite, *ibid.* **B158**, 469 (1979).
[14]M. B. Halpern, Phys. Rev. D **19**, 517 (1979).
[15]G. G. Batrouni, Nucl. Phys. **B208**, 467 (1982).
[16]M. C. Huang, R. L. Coldwell, and M. W. Katoot, Nucl. Phys. **B309**, 733 (1988).
[17]S. A. Chin, O. S. Van Rossmalen, G. A. Umland, and S. E. Koonin, Phys. Rev. D **31**, 3201 (1985).
[18]S. A. Chin, C. Long, and D. Robson, Phys. Rev. Lett. **57**, 2779 (1986).
[19]M. C. Huang and M. W. Katoot, Phys. Lett. (to be published).
[20]J. B. Kogut, D. K. Sinclair, R. B. Pearson, J. L. Richardson, and J. Shigemitsu, Phys. Rev. D **23**, 2945 (1981); J. B. Kogut and D. K. Sinclair, *ibid.* **24**, 1610 (1981).
[21]D. Gross and E. Witten, Phys. Rev. D **21**, 446 (1980).
[22]D. Horn and M. Karliner, Nucl. Phys. **B235**, 135 (1984).
[23]D. Horn, M. Karliner, and M. Weinstein, Phys. Rev. D **31**, 2589 (1985).
[24]G. Munster and P. Weisz, Nucl. Phys. **B180**, 13 (1981).
[25]B. Berg, A. Billoire, and C. Rebbi, Ann. Phys. (N.Y.) **142**, 185 (1982); G. Bhanot and C. Rebbi, Nucl. Phys. **B180**, 469 (1981).
[26]A. Hasenfratz and P. Hasenfratz, Phys. Lett. **93B**, 165 (1980).
[27]S. A. Chin, C. Long, and D. Robson, Phys. Rev. Lett. **57**, 2779 (1986).
[28]S. A. Chin and M. Karliner, Phys. Rev. Lett. **58**, 1803 (1987).
[29]M. Fukugita, T. Kaneko, T. Niuya, and A. Ukawa, Phys. Lett. **134B**, 341 (1984); **137B**, 444 (1984).
[30]T. A. DeGrand and C. Peterson, Phys. Rev. D **34**, 3180 (1986).
[31]B. A. Berg and A. H. Billoire, Phys. Rev. D **40**, 550 (1989).
[32]K. Ishikaw, M. Teper, and G. Schierholz, Phys. Lett. **110B**, 399 (1982).
[33]M. Abramowitz and I. A. Stegun, *Handbook of Mathematical Functions* (Dover, New York, 1972).